THE BELL SYSTEM TECHNICAL JOURNAL
Vol. 56, No. 8, October 1977
Printed in U.S.A.

Coupled Surface-Acoustic-Wave Resonators

By P. S. CROSS and R. V. SCHMIDT

(Manuscript submitted March 18, 1977)

Coupled Surface-Acoustic-Wave (SAW) grating resonators are investigated analytically with a transmission-matrix technique, and the measured frequency responses at ~145 MHz of devices on YZ-$LiNbO_3$ with Ti-diffused gratings are compared with the theoretical results. Coupled-mode theory is applied to derive the two-by-two transmission matrix relating the acoustic wave amplitudes at the input and output of a surface wave grating. Using the transmission matrices, the external transmission through a SAW resonator is found by matrix multiplication. Some fundamental aspects of resonator passband synthesis are introduced by considering the transmission through several acoustically cascaded resonators. Resonator filters where the transducers couple directly to the resonant cavities are treated by developing a description of the transducer that is compatible with the transmission matrix of the grating. The analysis technique is then applied to the familiar two-port resonator-filter. Next, coupled resonator-pairs with a transducer in each cavity are considered in detail for: (i) collinear acoustic coupling, (ii) multistrip coupling, and (iii) transducer coupling. Experimental results are presented for each configuration considered and good agreement with the analytical description is found in each case.

I. INTRODUCTION

Surface-acoustic-wave resonators are now well established as one-pole, narrowband filters in the frequency range 30 to 1000 MHz.[1,2] Recent work[3–10] has shown that multipole filters can be formed by coupling several resonators. In general, multipole filter responses can be synthesized by using one or more of the three established coupling mechanisms: (*i*) collinear acoustic coupling,[3–5] (*ii*) acoustic directional coupling (multistrip coupler),[6,7] or (*iii*) electrical coupling using transducers.[8–10]

Examples of two-pole resonator filters using the three types of cavity-coupling mechanisms are presented in Fig. 1. In each configuration,

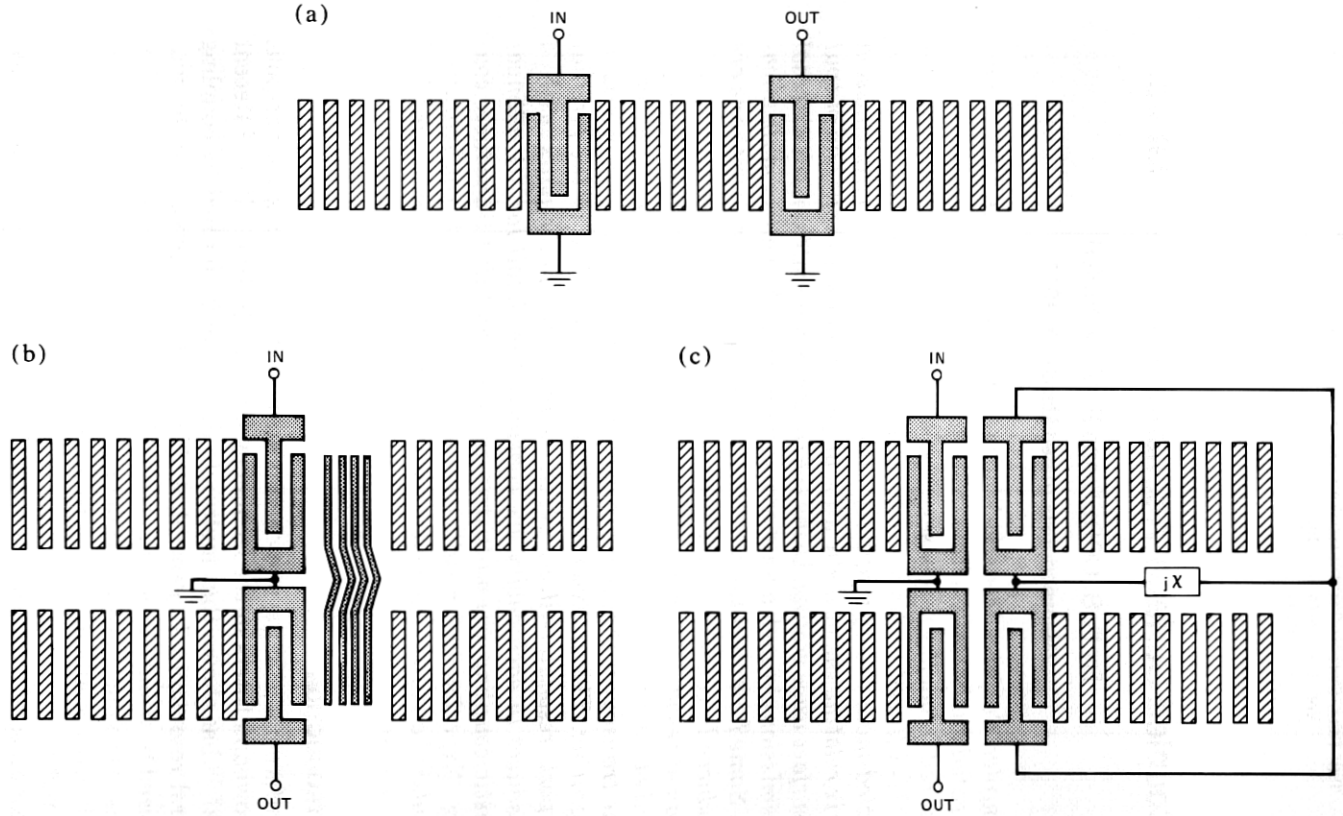

Fig. 1—Diagram of two-pole, coupled resonator filters using (a) collinear acoustic coupling, (b) multistrip coupling, and (c) transducer coupling with an external shunt susceptance.

there are two resonant cavities with a transducer in each cavity for coupling to the external circuitry.

In the collinear cascade structure the central grating, common to both cavities, is the coupling element. The strength of the central grating determines how much power can "leak" from one cavity to the other.

When either multistrip or transducer coupling is employed, each cavity has a distinct set of gratings, and the resonators are conveniently arranged in parallel with the acoustic power flowing in two separate "tracks." Coupling with the multistrip is effected by simply extending the electrodes of the coupler into both cavities. The degree of multistrip coupling is determined by the length or, equivalently, the number of electrodes of the coupler.

In the transducer-coupling configuration, a second transducer is placed in each cavity. The cavities are then coupled by connecting the transducers together, either directly or through an external electrical network. The external network provides a means for adjusting both the strength and phase of the cavity coupling.

In order to design a filter using coupled grating resonators it is necessary to be able to relate the frequency response of the filter to the parameters describing the gratings, transducers, and coupling elements. We present here a general technique for obtaining the frequency response of coupled resonators. In addition, the technique yields closed-form expressions for the insertion loss, out-of-band response and the near-in-band shape which aid in filter design.

The approach taken in this paper is to first develop the transmission matrix of a uniform grating and use it to analyze the external transmission response of a single resonator. Next, the properties of coupled resonators are introduced by studying the external transmission response of acoustically cascaded resonators.

We then present a description of the interdigital transducer which is compatible with the transmission matrix description of the gratings. With this description one can calculate the transmission response of any resonator structure which includes internal transducers.

The technique is applied to the familiar two-port resonator-filter. Then coupled-resonator pairs are treated in detail for each of the three cavity-coupling mechanisms. Experimental results at ~145 MHz are presented for each configuration considered, and the good agreement with theory that is found in each case substantiates the analytical models.

II. GRATING TRANSMISSION MATRIX

In this section, the transmission matrix of a surface-wave grating is derived. A transmission matrix relates the forward and backward traveling-wave-amplitudes at the left side of an element to those on the right

side. It is therefore useful to establish a compact notation by introducing the vector

$$\mathbf{W}_i = \begin{bmatrix} w_i^+ \\ w_i^- \end{bmatrix} \tag{1}$$

which represents the complex amplitudes of the forward-, w_i^+, and backward-, w_i^-, traveling waves at the right-hand reference plane of the ith element of a filter structure. The amplitudes have dimensions of $\sqrt{\text{Power}}$. Thus, the transmission characteristics of the ith element of the structure are described by the matrix equation

$$\mathbf{W}_{i-1} = \mathcal{M}_i \mathbf{W}_i \tag{2}$$

where $\mathcal{M}_i$ is the 2×2 transmission matrix of the ith element.

The transmission matrix of a grating is derived using a plane-wave, coupled-mode analysis which was originally applied to thick holograms[11] and subsequently to distributed feedback lasers[12,13] and acoustic grating reflectors.[3] The grating to be analyzed is taken to have constant period Λ, and to extend from $x = -L$ to $x = 0$. Near the Bragg frequency, only the fundamental Fourier component of the grating perturbation provides phase-matching between the forward- and backward-traveling waves. Thus, in the analysis, a lossless grating is mathematically modeled by a sinusoidal velocity perturbation given by

$$v(x) = v_0 - \frac{\Delta v}{2} \cos(Kx) \tag{3}$$

where $K = 2\pi/\Lambda$. Furthermore, we assume that the surface wave propagation can be represented by the scalar wave equation

$$\frac{d^2\Psi}{dx^2} + \frac{\omega^2}{v^2(x)}\Psi = 0 \tag{4}$$

where ω is the surface-wave radian frequency. The scalar Ψ represents the quasistatic electric potential at the surface of the piezoelectric crystal associated with the surface wave. The general solution[11] of eq. (4) is

$$\Psi(x) = w^+(x) + w^-(x) \tag{5a}$$

where

$$w^+(x) = \psi^+(x)e^{-j\beta_0 x} \tag{5b}$$

$$w^-(x) = \psi^-(x)e^{+j\beta_0 x} \tag{5c}$$

are respectively the forward and backward wave amplitudes in the grating and $\beta_0 = \pi/\Lambda$ is the propagation constant of the surface wave at the Bragg frequency $\omega_0 = \pi v_0/\Lambda$. By appropriately combining eqs. (3) through (5) and dropping higher harmonic terms one obtains the coupled

wave equations

$$-\frac{d\psi^+}{dx} - j\delta\psi^+ = j\frac{\beta}{\beta_0}\kappa\psi^- \tag{6a}$$

$$\frac{d\psi^-}{dx} - j\delta\psi^- = j\frac{\beta}{\beta_0}\kappa\psi^+ \tag{6b}$$

where $\beta = \omega/v_0$, $\kappa = (\beta/4)\cdot\Delta v/v_0$ is the grating coupling coefficient and

$$\delta = \frac{\beta^2 - \beta_0^2}{2\beta_0} \tag{7}$$

is a measure of the frequency deviation from the Bragg frequency. For high-Q resonators, we are particularly interested in a limited frequency range such that $\beta/\beta_0 \approx 1$ and the coupled wave equations can be simplified by setting $\beta/\beta_0 = 1$ and letting $\delta = (\omega - \omega_0)/v_0$. In the remainder of this paper we use this narrowband approximation. The exact forms of (6) must be used if responses over large bandwidths are required.

Solving eqs. (3) through (7) for the wave amplitudes at $x = -L$ in terms of the wave amplitudes at $x = 0$ yields the following transmission relation

$$\mathbf{W}(-L) = \mathcal{G}\mathbf{W}(0) \tag{8a}$$

where the transmission matrix $\mathcal{G}$ for a grating an integral number of periods long is given by

$$\mathcal{G} = (-1)^{N_g}\frac{\cosh(\sigma L)}{\sqrt{1-\Delta^2}} \times \begin{bmatrix} \sqrt{1-\Delta^2} + j\Delta\tanh(\sigma L) & j\tanh(\sigma L) \\ -j\tanh(\sigma L) & \sqrt{1-\Delta^2} - j\Delta\tanh(\sigma L) \end{bmatrix} \tag{8b}$$

where

$$N_g = L/\Lambda, \tag{8c}$$

$$\sigma = \sqrt{\kappa^2 - \delta^2} = \kappa\sqrt{1-\Delta^2} \tag{8d}$$

and

$$\Delta = \delta/\kappa \tag{8e}$$

is the normalized frequency deviation.

The reflection coefficient, Γ, at the plane $x = -L$ for a wave incident from the left is

$$\Gamma(\Delta) = \frac{w^-(-L)}{w^+(-L)} = \frac{-j}{\sqrt{1-\Delta^2}\coth(\sigma L) + j\Delta} \tag{9}$$

and at the Bragg frequency, $\Delta = 0$,

$$\Gamma(0) = -j\rho \tag{10}$$

where $\rho = \tanh(\kappa L)$.

The grating transmission matrix and reflection coefficient have been derived by postulating a sinusoidal velocity perturbation grating. The final expressions are, however, in terms of a coupling coefficient, κ, which describes the strength of the perturbation that forms the grating. By appropriately identifying the coupling coefficient of other grating types (such as surface corrugations), the grating transmission matrix (8b) describes the behavior of surface-wave gratings formed with any perturbation mechanism.

Equations (9) and (10) provide a means for experimentally determining the coupling coefficient for a particular physical grating. It has been found[14] that κ can be obtained by either measuring the reflectivity at $\delta = 0$ and using (10) or by measuring the fractional bandwidth $\Delta\omega/\omega_0$ between reflection zeros and calculating κ from the expression

$$\kappa = \frac{\pi}{2\Lambda}\sqrt{\left(\frac{\Delta\omega}{\omega_0}\right)^2 - \left(\frac{2\Lambda}{L}\right)^2} \tag{11}$$

obtained from (9). The first method is most suitable for weakly reflecting gratings while the second method works best on highly reflective gratings.

For the specific case of shallow-groove gratings, one can use, in addition to the above techniques, the results of Li *et al.*[15,16] to determine the coupling coefficient which gives $\kappa = h/3\Lambda^2$ for corrugations of depth h. The various second-order effects associated with stored reactive energy have been neglected here for simplicity.

The phase of the reflection coefficient and the off-diagonal terms of the transmission coefficient depend on the choice of grating reference planes. In Appendix A, the question of specifying reference planes is treated in detail, and it is shown that reference planes can be found for any grating such that the transmission matrix in (8b) is applicable.

If the ith element of the structure is a transmission line extending from $x = -L_i$ to $x = 0$, it is described by the familiar transmission equation

$$\mathbf{W}_{i-1} = \Phi_i \mathbf{W}_i \tag{12}$$

where

$$\Phi_i = \begin{bmatrix} e^{j\beta L_i} & 0 \\ 0 & e^{-j\beta L_i} \end{bmatrix}. \tag{13}$$

Thus far, the surface-wave gratings have been treated as lossless. However, in many circumstances, small grating losses have a significant

influence on the grating filter transmission response. In Appendix A, the transmission matrix of a lossy grating with a distributed attenuation coefficient, α, is given in eq. (82). This matrix is unnecessarily complicated when only frequencies near the Bragg frequency, $|\Delta| \ll 1$, are considered. An approximate transmission matrix for a lossy grating can be considered when $\alpha/\kappa \ll 1$ and $\Delta \ll 1$ by decomposing the lossy matrix (82) at $\Delta = 0$ as follows:

$$\mathcal{G} \simeq \mathcal{A}\mathcal{F}\mathcal{A} \tag{14a}$$

where

$$\mathcal{A} = \begin{bmatrix} \exp\left(\frac{\alpha\rho}{2\kappa}\right) & 0 \\ 0 & \exp\left(-\frac{\alpha\rho}{2\kappa}\right) \end{bmatrix} \tag{14b}$$

$$\mathcal{F} = \left(1 + \frac{\Delta^2}{2}\right)\cosh(\kappa L)\begin{bmatrix} 1 - \frac{\Delta^2}{2} + j\Delta\rho & j\rho \\ -j\rho & 1 - \frac{\Delta^2}{2} - j\Delta\rho \end{bmatrix} \tag{14c}$$

where, as before $\rho = \tanh(\kappa L)$ and $\Delta = \delta/\kappa$. This decomposition is equivalent to placing a lumped, frequency-independent loss[17] at each side of the grating. The matrix $\mathcal{F}$ is the lossless grating transmission matrix (8b) simplified for the condition $|\Delta| \ll 1$ and N_g even. The decomposition of $\mathcal{G}$ in (14) has two advantages. First, other loss mechanisms (such as bulk radiation loss) that are localized in nature can be mathematically included as a component of α. And, second, the important frequency dependence of $\mathcal{G}$ is all contained in $\mathcal{F}$ so that the simplified matrix $\mathcal{F}$ can be used to obtain closed-form expressions for the resonant passband shape of a given structure.

III. TRANSMISSION RESPONSE OF CASCADED GRATING STRUCTURES

The transmission matrices derived in Section II provide the means to calculate the properties of cascaded structures of gratings and transmission lines. As an example of the application of the transmission matrices, we first consider a grating resonator as illustrated in Fig. 2a. The resonator consists of two identical gratings each of length L, which are separated by a quarter-wave transmission line. The wave amplitudes $\mathbf{W}_0$ and $\mathbf{W}_3$, at the left and right reference planes respectively, are related by the matrix equation

$$\mathbf{W}_0 = \mathcal{G}_1\Phi_2\mathcal{G}_3\mathbf{W}_3 \equiv \mathcal{R}\mathbf{W}_3 \tag{15}$$

where $\mathcal{G}_1 = \mathcal{G}_3$ are the transmission matrices of the first and third elements (gratings) and Φ_2 is the transmission matrix of the second element

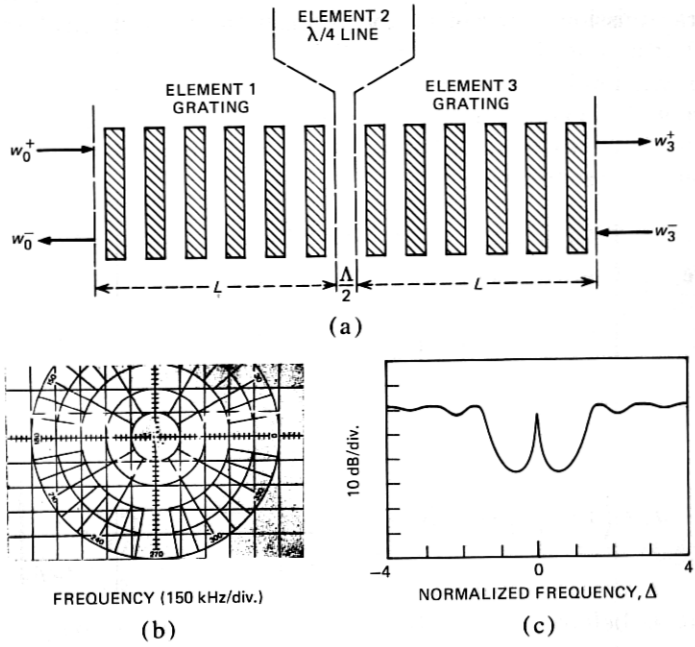

Fig. 2—(a) Diagram of a grating resonator in the external transmission configuration. (b) The transmission spectrum at ~145.5 MHz for a resonator on YZ-$LiNbO_3$ using Ti-diffused gratings with $\Lambda = 12$ μm and L = 6.48 mm. (c) The calculated transmission spectrum for the device in (b) using $\kappa = 3.74$ cm^{-1} and $\alpha = 0.036$ cm^{-1}.

(in this case a quarter-wave line). The matrix $\mathcal{R}$ is the transmission matrix of the resonator.

In the laboratory, the external power transmission, $|w_3^+/w_0^+|^2$, through the structure of Fig. 2a is the most conveniently measured quantity. A typical experimental transmission spectrum for a resonator formed by Ti-diffused gratings[14] in YZ-$LiNbO_3$ is shown in Fig. 2b. Far off resonance, where the gratings are transparent, the transmission is near unity. Inside the grating stopband, the gratings are highly reflective and there is a deep transmission minimum. Near resonance, there is once again near-unity transmission.

The theoretical transmission response can be obtained by applying the boundary condition $w_3^- = 0$ to eq. (15). The external power transmission is then

$$\left|\frac{w_3^+}{w_0^+}\right|^2 = \frac{1}{R_{11}R_{11}^*} \tag{16}$$

where R_{11} is the 11 element of the $\mathcal{R}$ matrix of (15). In Fig. 2c, the calculated spectrum is given for the structure of Fig. 2b where α and κ are

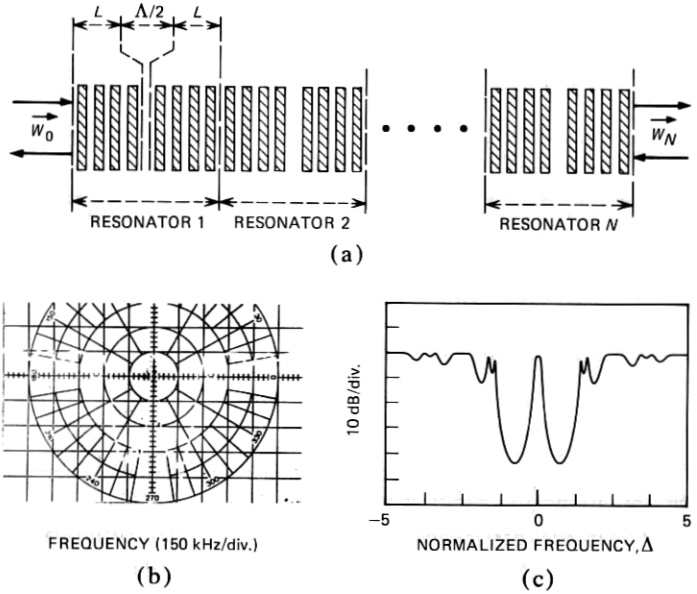

Fig. 3—(a) Diagram of a cascade of N identical resonators. (b) The transmission spectrum at 145.5 MHz of a cascade of three identical resonators with $\Lambda = 12\ \mu m$ and $L = 3.84$ mm. (c) The calculated transmission spectrum for the device in (b) using $\kappa = 3.55\ cm^{-1}$ and $\alpha = 0.027\ cm^{-1}$.

chosen to fit the insertion loss and stopband width. The complete grating transmission matrix of eq. (82) in Appendix A is used in the calculation.

In many cases, only the frequency response near resonance is of interest and the external power transmission can be found using the approximate grating transmission matrix (14a). Under the conditions $|\delta|$, $\alpha \ll \kappa$ and $2\cosh(\kappa L) \approx \exp(\kappa L)$, eq. (16) simplifies to

$$\left|\frac{w_3^+}{w_0^+}\right|^2 = \frac{1}{1 + \frac{\alpha}{\kappa}\exp(2\kappa L) + \frac{\delta^2 + \alpha^2}{4\kappa^2}\exp(4\kappa L)} \tag{17}$$

From (17), an analytical expression for the unloaded resonator quality factor, Q_u, can be obtained and is given by

$$\frac{1}{Q_u} = \frac{1}{Q_r} + \frac{1}{Q_g} \tag{18}$$

where

$$Q_r = \frac{\pi}{\kappa\Lambda}\sinh^2(\kappa L) \simeq \frac{\pi}{4\kappa\Lambda}\exp(2\kappa L) \tag{19}$$

is the Q associated with radiation loss from the ends of the gratings and

$$Q_g = \frac{\pi}{2\alpha\Lambda} \tag{20}$$

is the Q associated with the distributed internal grating loss (material losses, surface imperfections, and diffraction).

The distributed internal grating loss can be determined from the resonant transmission loss through the resonator. From eq. (17) the resonant transmission is

$$\left|\frac{w_3^+}{w_0^+}\right|^2 = \frac{1}{\left[1 + \frac{1}{2}\frac{\alpha}{\kappa}\exp(2\kappa L)\right]^2} \tag{21}$$

from which α can be determined.

The transmission matrix analysis technique is easily extended to more complicated structures such as those that are encountered in multipole filter-synthesis applications. The simple case of a collinear cascade of identical resonators shown in Fig. 3a provides an illustrative example since such a cascade has been shown to have a near-resonance transmission response described by a Chebyshev polynominal.[3,4,18] The transmission matrix of a cascade of N lossless, identical resonators is given by $(\mathcal{R})^N$ where $\mathcal{R}$ is the transmission matrix of a single resonator. If the lossless grating transmission matrix (8b) is used, the following expression for $\mathcal{R}$ is found:

$$\mathcal{R} = \mathcal{G}\Phi\mathcal{G} = \begin{bmatrix} \frac{2\Delta}{\sqrt{1-\Delta^2}}SC - j\left[1 - 2\frac{\Delta^2}{1-\Delta^2}S^2\right] & -j\frac{2\Delta}{1-\Delta^2}S^2 \\ j\frac{2\Delta}{1-\Delta^2}S^2 & \frac{2\Delta}{\sqrt{1-\Delta^2}}SC + j\left[1 - 2\frac{\Delta^2}{1-\Delta^2}S^2\right] \end{bmatrix} \tag{22}$$

where $S = \sinh(\sigma L)$ and $C = \cosh(\sigma L)$. Equation (22) is applicable over the region of validity of the coupled-mode approximation, $|\Delta| \ll \pi/\kappa\Lambda$.

Using the results of Storch[19] to evaluate $(\mathcal{R})^N$, one can obtain the following expression for the transmission response through the cascade:

$$\left|\frac{w_N^+}{w_0^+}\right|^2 = \frac{1}{\left[1 + 2\frac{\Delta}{1+\Delta^2}S^2U_N(\xi)\right]^2} \tag{23}$$

where

$$\xi = \frac{2\Delta}{\sqrt{1-\Delta^2}} CS$$

and U_N is the Chebyshev polynominal of the second kind of Nth order. Near the resonant frequency the response is simplified to

$$\left|\frac{w_N^+}{w_0^+}\right|^2 \approx \frac{1}{1+\Omega^2 U_N^2(\Omega)} \tag{24}$$

where $\Omega = 2Q_r(\omega - \omega_0)/\omega_0$ and Q_r is the radiation Q of a single resonator. In Fig. 3b the experimental transmission response of a cascade of three coupled resonators is presented, and in Fig. 3c, the theoretical frequency response calculated using the lossy grating matrix (82) is given. The theoretical description again provides an excellent fit to the data.

The comparisons made in this section between the experimental and theoretical transmission spectra of cascaded grating structures provide a quantitative verification of the analytical model and approximations presented in Section II. In particular, over the frequency range used in the measurements ($\Delta\beta/\beta \lesssim 1$ percent), the excellent agreement between the calculated and experimental responses justifies both the use of the coupled mode equations and the narrow-band ($\beta/\beta_0 \simeq 1$) simplification. It should also be noted that the loss coefficient required to theoretically fit the data is only about twice the surface wave propagation loss of $LiNbO_3$. Thus, the titanium diffusion process[14] produces a low-loss surface perturbation that is ideal for high-Q resonators.

IV. INTRACAVITY TRANSDUCERS AND THE TWO-PORT RESONATOR

In the preceding sections, coupled-mode theory has been applied to derive a transmission matrix description of SAW gratings and resonators. The resonators become useful bandpass filters with low out-of-band transmission, when the transducers are placed inside the cavity.[20–22] In Fig. 4 an interdigital transducer (IDT) is depicted schematically and the various physical quantities associated with the IDT are indicated. The quantities $w_i^{\pm}$ and $w_{i-1}^{\pm}$ are the local amplitudes of the various acoustic waves as previously defined, and a_i and b_i are the amplitudes of the electrical waves incident and emanating from the transducer, respectively.

The terminal amplitudes at the transducer can be related by a dimensionless matrix $\mathcal{T}$, such that

$$\begin{pmatrix} w_{i-1}^+ \\ w_{i-1}^- \\ b_i \end{pmatrix} = \mathcal{T} \begin{pmatrix} w_i^+ \\ w_i^- \\ a_i \end{pmatrix} \tag{25}$$

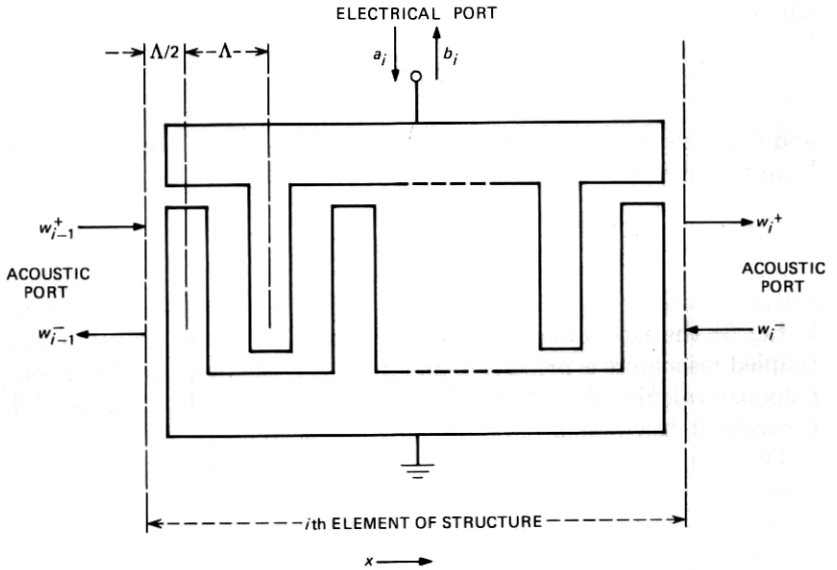

Fig. 4—Diagram of an interdigital transducer.

where $\mathcal{T}$ is given by

$$\mathcal{T} = \begin{pmatrix} t_{11} & t_{12} & t_{13} \\ -t_{12} & t_{22} & t_{23} \\ st_{13} & -st_{23} & t_{33} \end{pmatrix} \tag{26}$$

and s is a symmetry parameter expressing whether the transducer has an even ($s = 1$) or odd ($s = -1$) number of electrodes.

The transducer description of eq (25) has the useful property that the acoustic amplitudes are expressed in transmission matrix form. As a result, (25) is conveniently decomposed into two equations:

(i) The acoustic amplitudes at the transducer reference planes are related by

$$\mathbf{W}_{i-1} = t_i \mathbf{W}_i + a_i \tau_i \tag{27}$$

where t_i is the transmission matrix

$$t_i = \begin{pmatrix} t_{11} & t_{12} \\ -t_{12} & t_{22} \end{pmatrix}_i \tag{28}$$

and τ_i is the input coupling vector

$$\tau_i = \begin{pmatrix} t_{13} \\ t_{23} \end{pmatrix}_i \tag{29}$$

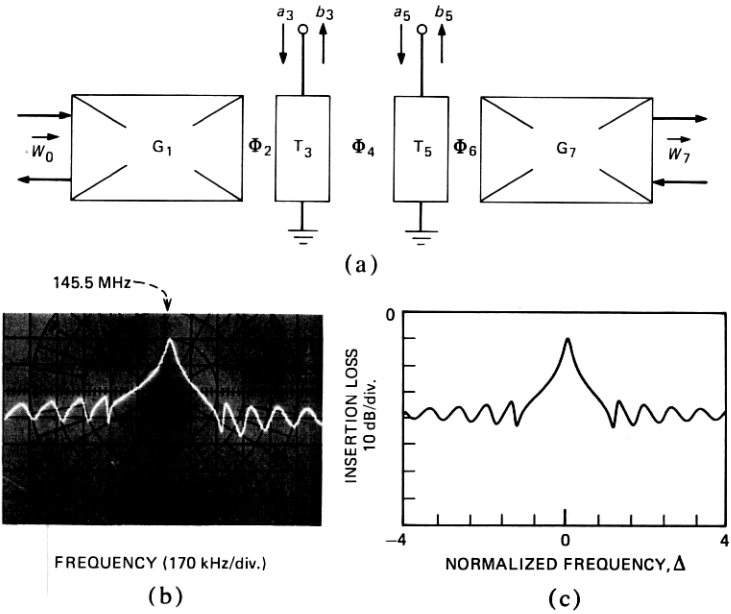

Fig. 5—(a) Diagram of a two-port resonator. (b) The electrical transmission spectrum for a two-port resonator on YZ-$LiNbO_3$ with gratings 9.6 mm long and 12 μm period, optimally placed transducers with $N_t = 5$, $Z_e = 50\ \Omega$, and an acoustic aperture of 50 wavelengths. (c) The calculated spectrum for the device in (b) using $\kappa = 4.5\ \text{cm}^{-1}$, $\alpha/\kappa = 0.01$, $R_s = 11\ \Omega$, $\epsilon = 0.04$, and $\phi_4 = 9.98\ \pi$ on resonance.

(*ii*) The electrical signal leaving the transducer is expressed by

$$b_i = \boldsymbol{\tau}_i' \cdot \mathbf{W}_i + a_i(t_{33})_i \tag{30}$$

where $\boldsymbol{\tau}_i'$ is an output coupling vector

$$\boldsymbol{\tau}_i' = s \begin{pmatrix} t_{13} \\ -t_{23} \end{pmatrix}_i \tag{31}$$

The symbol · in (30) indicates the scalar (dot) product.

As shown in Appendix B, eqs. (27) and (30) allow the analysis of resonators and coupled-resonators to be reduced to a simple, matrix-multiplication algorithm.

The elements of the matrix $\mathcal{T}$ are evaluated by using an appropriate transducer model.[23,24] The accuracy of the matrix elements depends on the degree of sophistication of the model used. For example, the Mason equivalent circuit model first used for interdigital transducers by Smith[23] *et al.* has proven very useful in practice. The complete matrix $\mathcal{T}$ based on the Smith-Mason model is given in Appendix B.

In many resonator applications, however, only a first-order analysis is required. Thus, by neglecting the static transducer capacitance and

the frequency dependence of the propagation phase-shift through the transducer, $\mathcal{T}$ is given by

$$(\mathcal{T})_{\text{first-order}} \approx s \begin{bmatrix} 1+g+g_s & -g-g_s & s\sqrt{2g} \\ g+g_s & 1-g-g_s & s\sqrt{2g} \\ \sqrt{2g} & -\sqrt{2g} & s \end{bmatrix} \tag{32}$$

where

$$g = G_r Z_e \tag{33}$$

$$g_s = G_r R_s \tag{34}$$

and G_r, Z_e, and R_s are the transducer radiation conductance, load resistance, and series electrode resistance, respectively. The first-order matrix in eq. (32) is sufficient for calculating the near-resonance properties of many SAW resonators, but the more complete matrix in eq. (84) is required for wideband descriptions.

As a first application of the transducer matrix in (32) and of the matrix-multiplication algorithm in Appendix B, consider the two-port resonator in Fig. 5a. Ideally, the transducers are optimally-placed[25] ($\phi_2 = \phi_6 = \pi/4$), and the cavity is resonant at $\Delta = 0$ ($\phi_4 = m\pi$). Thus, from eq. (32) and eqs. (96)–(103), the electrical power-transmission factor P_{53} of the optimal two-port is given by

$$P_{53} = \left|\frac{b_5}{a_3}\right|^2 = \left|\frac{2g}{2g + 2g_s + \dfrac{1-r}{1+r}}\right|^2 \tag{35}$$

where, $r = j\Gamma$, Γ is the frequency-dependent reflection coefficient of each grating (G_1 is assumed to be identical to G_7), and g and g_s are given in eqs. (33) and (34), respectively.

The total loading on the cavity can be separated into two components: (*i*) the power coupled to external circuit and (*ii*) the power lost in the filter structure.

Thus, eq. (35) can be written in the more intuitively recognizable form

$$P_{53} = \left|\frac{\mu_C}{\mu_C + \mu_L}\right|^2 \tag{36}$$

where

$$\mu_C = 8g \tag{37}$$

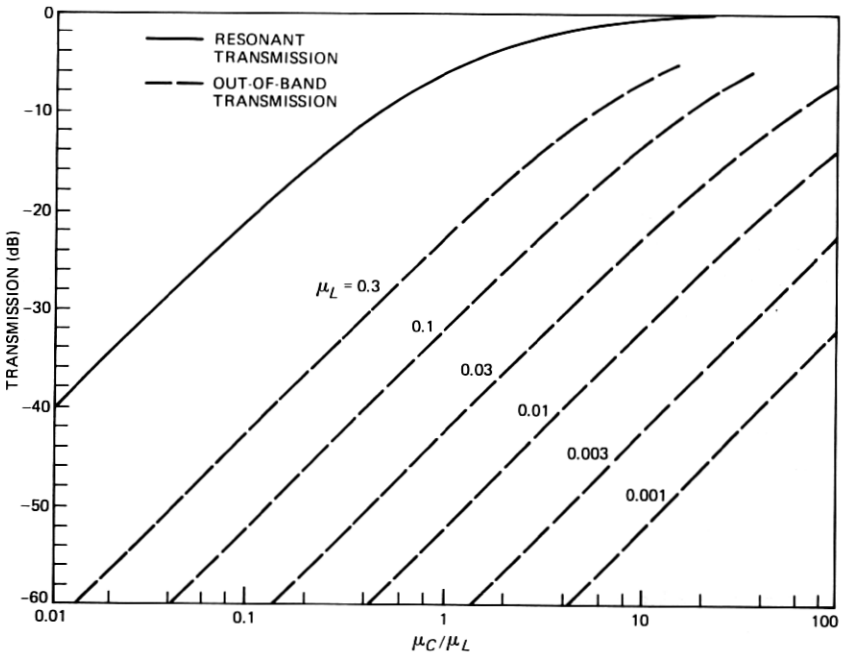

Fig. 6—Nomogram giving the resonant and out-of-band transmission for two-port, surface-acoustic-wave grating resonators and matched grating resonator pairs. The resonant transmission is determined by the ratio of the transducer cavity loading μ_C to the cavity loading μ_L due to all other mechanisms. The out-of-band transmission is only a function of μ_C. The dashed curves are contours of out-of-band transmission for constant cavity loss. The resonant and out-of-band transmission can be found from μ_C and μ_L or vice-versa. The nomogram is directly applicable to single resonators and matched collinearly coupled resonator pairs. To use the nomogram with matched multistrip-coupled pairs, multiply the ordinate by $4\nu_m^2|\Gamma|^2$ (see Section VII) and for matched transducer-coupled cavities, multiply the ordinate by $(\nu_t/4)^2$ (see Section VIII).

is the single-transit, fractional power coupling to the external circuit and

$$\mu_L = 8g_s + 4(1 - r)/(1 + r) \tag{38}$$

is the single-transit, fractional power loss due to all other mechanisms (ohmic loss, bulk scattering, intrinsic propagation losses, and transmission through the gratings). Note that in the optimal resonator described here, the transducers are spaced an integral number of half wavelengths apart so that coherent interactions take place that allow μ_C to be greater than 1 for strong-coupling transducers.

On resonance ($\Delta = 0$), for highly reflective gratings [$\exp(2\kappa L) \gg 1$], eq. (38) becomes

$$\mu_L \approx 8g_s + 2\epsilon + 2\alpha/\kappa + 4\exp(-2\kappa L) \tag{39}$$

where ϵ is a localized[17] excess loss that accounts for mode-conversion losses. By dividing the numerator and denominator in eq. (36) by μ_L^2, the

resonant power transmission through a resonator is described by the single parameter μ_C/μ_L.

Figure 6 is a nomogram for finding the resonant and out-of-band transmission of grating resonators. The solid curve is the resonant insertion loss versus μ_C/μ_L. Plotted with dashed curves is the out-of-band transmission with the cavity loss μ_L as a parameter. Using the nomogram, the resonant and out-of-band transmission can be found knowing μ_C and μ_L or vice versa. The nomogram is also applicable to coupled resonators as described in the caption to Fig. 6 and in Sections VI, VII, and VIII. Coldren and Rosenberg[6,17] have used similar diagrams for the resonant insertion loss of single and multistrip-coupled resonators as a function of coupling and loss parameters.

Equation (35) can also be used to find the loaded electrical Q, Q_{Le_1}, of a single-cavity, two-port resonator. For $\exp(2\kappa L) \gg 1$, it is found that

$$Q_{Le_1} = \frac{\pi}{\kappa\Lambda} \frac{1}{(\mu_C + \mu_L)} \tag{40}$$

where $\pi/\kappa\Lambda$ is the single-transit cavity phase-shift.

The algorithm used to derive eq. (35) provides a flexible tool for interpreting experimental device performance, since a large number of electrical, mechanical, and geometrical properties are explicitly contained in the analysis. For example, consider the transmission response in Fig. 5b of a two-port resonator with Ti-diffused gratings on YZ-$LiNbO_3$. The resonant insertion loss is 10 dB, and from eq. (36) or Fig. 6,

$$\frac{\mu_C}{\mu_L} = 0.46 \tag{41}$$

Next, the transducers each have five electrodes 50 wavelengths long, and, from eqs. (33), (93), and (94),

$$\mu_C = 0.052 \tag{42}$$

for $Z_e = 50\Omega$. From (41) and (42), it is found that

$$\mu_L = 0.112 \tag{43}$$

The transmission minima on each side of the resonance occur near the first reflection zeroes of the gratings. Thus, eq. (11) can be used to estimate κ, with the result

$$\kappa \approx 4.3 \text{ cm}^{-1} \tag{44}$$

The gratings are each 0.96 cm long (800 Λ), and from eq. (44),

$$e^{-2\kappa L} = 0.00026 \tag{45}$$

From external transmission measurements on resonators (see Sections II and III), the loss α/κ associated with diffused gratings is found to be ~0.01. Thus, from (39)–(45), the remaining loss is probably associated with the transducers and is given by

$$8g_s + 2\epsilon = \mu_L - \frac{2\alpha}{\kappa} - 4e^{-2\kappa L} = 0.092 \tag{46}$$

The electrode resistance ($R_s = 11\ \Omega$) is calculated from the metal thickness (2700 Å of aluminum),

$$g_s = 0.0014 \tag{47}$$

and, finally, from eqs. (46) and (47)

$$\epsilon = 0.040 \tag{48}$$

The 4 percent excess loss ϵ is probably due to bulk mode conversion by the transducer electrodes. Both loss mechanisms associated with the transducers (series resistance and bulk mode conversion) should be less significant on low-coupling materials such as ST-quartz due to the increased transducer length.

In order to complete the description of the resonator in Fig. 5a, the phase-shifts ϕ_2, ϕ_4, and ϕ_6 must be specified. It is observed in practice that the velocity of propagation is very sensitive to surface perturbations (piezoelectric-loading, mass-loading, and reactive energy storage). As a result, the separation between the gratings must be empirically adjusted to compensate for the velocity variations in the structure. For the device of Fig. 5b, the appropriate empirical values are $\phi_2 = \phi_4 = \pi/4$ and $\phi_6 = 9.98\ \pi$ on resonance.

The parameters estimated in (41)–(48) have been used with the algorithm in Appendix B to calculate the complete transmission spectrum shown in Fig. 5c.

V. COUPLED GRATING-RESONATORS—GENERAL CONSIDERATIONS

Multipole filters are formed by coupling together two or more cavities. The general configuration for a cascade-coupled multipole resonator-filter is shown in Fig. 7. Acoustic energy is launched by the transducer in the input cavity, propagates through the coupling structure C_5, and is detected by the transducer in the output cavity. The coupling structure C_5 consists in general of some combination of gratings, phase shifts, transducers, and multistrip couplers. The overall filter response is determined by the properties of C_5 as well as the properties of the input and output cavities.

In order to better understand the various elements that can be used in the coupling structure C_5, two-pole resonators formed by acoustic collinear coupling, multistrip coupling, and transducer coupling are

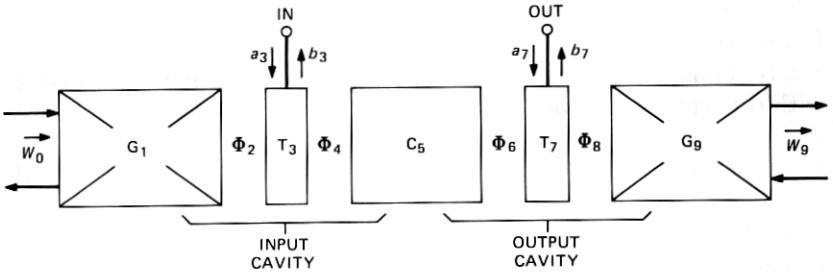

Fig. 7—Diagram of the configuration for cascade-coupled SAW grating resonators with an arbitrary coupling element, C_5.

discussed individually in the next three sections. It is shown for each coupling mechanism that the important, near-resonance properties of the coupling structure are expressed by the matrix $\hat{\mathcal{C}}$

$$\hat{\mathcal{C}} = \frac{1}{\nu}\begin{bmatrix} e^{j2\delta L_{\text{eff}}} & j\sqrt{1-\nu^2} \\ -j\sqrt{1-\nu^2} & e^{-j2\delta L_{\text{eff}}} \end{bmatrix} \tag{49}$$

where ν is a real parameter ≤ 1, and L_{eff} is the effective contribution to the cavity length by the coupling structure.

The parameter ν is the magnitude of the amplitude transmission coefficient through the coupling structure and is a measure of the degree of coupling between the cavities. The quantity $\exp(j2\delta L_{\text{eff}})$ is a propagation phase factor that accounts for the phase shift through the coupling structure.

The degree of coupling between the cavities (specified by ν) largely determines the transmission characteristics of the resonator pair. For example, using the method outlined in Appendix B, the resonant transmission of a pair of cavities is found to be

$$\left|\frac{b_7}{a_3}\right|^2_{\delta=0} = \frac{1}{4}\left|\frac{\nu\mu_C}{1+\left(\frac{\mu_C+\mu_L}{4}\right)^2 - \sqrt{1-\nu^2}\left[1-\left(\frac{\mu_C+\mu_L}{4}\right)^2\right]}\right|^2 \tag{50}$$

where the quantity $(\mu_C + \mu_L)$ is the single-transit, fractional power loading on the combined resonator pair. Equivalently, $(\mu_C + \mu_L)$ can be interpreted as the *round-trip* power loading on each cavity.

By differentiating eq. (50) with respect to ν, it is found that maximum, resonant transmission is obtained when the coupling structure "matches" [26] the two cavities according to

$$\nu_{\text{opt}} = \frac{1}{2}\frac{\mu_C+\mu_L}{1+\left(\frac{\mu_C+\mu_L}{4}\right)^2} \tag{51}$$

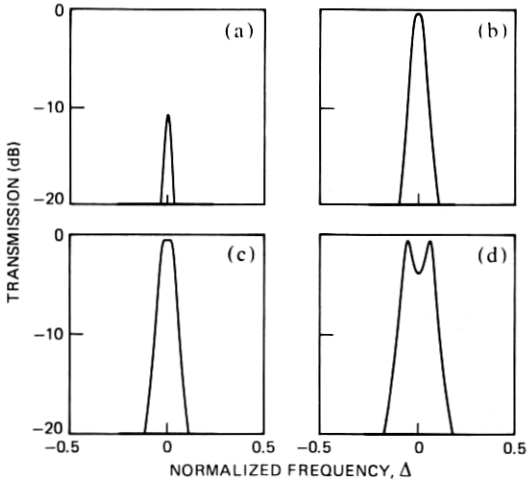

Fig. 8—Near-resonance transmission spectra for lossless, coupled resonator pairs that are: (a) undercoupled, (b) matched, (c) slightly overcoupled, and (d) overcoupled for maximum 3-dB bandwidth.

Qualitatively, the cavities are matched when the loading on each cavity due to the coupling structure is equal to the loading due to all other mechanisms.

The importance of matching the individual resonators in a coupled structure is illustrated in Fig. 8. If the parameter ν is too small, the cavities are *undercoupled* and there is a large resonant insertion loss as in Fig. 8a. When $\nu = \nu_{opt}$ from eq. (51), the cavities are *matched* and minimum insertion loss is obtained as shown in Fig. 8b. As ν is increased slightly beyond ν_{opt}, the peak flattens and broadens as in Figure 8c. For still larger values of ν the cavities become *overcoupled* and the resonance splits into two peaks as in Fig. 8d where the dip between peaks is 3 dB. Thus, the degree of cavity-coupling, ν, is a central parameter in determining the passband shape and insertion loss.

The matched condition (51) has a further interesting consequence. When the frequency dependence of the transfer function is included in (50), it can be shown for matched cavities that

$$\left|\frac{b_7}{a_3}\right|^2 \approx \left|\frac{\mu_C}{\mu_C + \mu_L}\right|^2_{\delta=0} \left[\frac{1}{1 + \Omega^2 U_2^2(\Omega)}\right] \tag{52}$$

where $U_2 = 2\Omega$ is the second Chebyshev polynomial of the second kind. The parameter Ω is a normalized frequency

$$\Omega = 2\frac{\Delta\omega}{\omega_0} Q_{Le_2} \tag{53}$$

where Q_{Le_2} is the loaded electrical Q of each cavity in the coupled pair.

The Chebyshev-polynomial form in eq. (52) is the same as the form obtained for a coupled pair of identical resonators in the external transmission configuration [see eq. (24)]. Although it is not rigorously proven here, eq. (52) indicates that the passband shapes that can be obtained in external transmission can also be obtained with intracavity transducers. Thus, the procedure for synthesizing resonant passbands can be simplified by first investigating the passband in the external transmission configuration, and subsequently including the transducers.

VI. COLLINEAR ACOUSTICALLY COUPLED RESONATORS

An acoustically coupled resonator pair is formed by inserting a section of grating between the input and output transducers as shown in Fig. 9a. Comparing Figs. 7 and 9a, the coupling structure in Fig. 9a is simply a section of grating. From eq. (14a), the near-resonance coupling matrix is given by

$$\mathcal{C} \approx \mathcal{A}\mathcal{F}\mathcal{A} \tag{54}$$

The loss matrix $\mathcal{A}$ in eq. (54) has the same form as that given in eq. (14b), but any excess loss due to the transducers must be included.

The near-resonance behavior of a highly reflective grating, described by the matrix $\mathcal{F}$, is approximately equal to the coupling matrix $\hat{\mathcal{C}}$ in eq. (49) when the identification

$$\nu_g = \operatorname{sech}(\kappa L_5) \tag{55}$$

is made and L_{eff} is the effective penetration depth into the grating, $1/2\kappa$. The quantity ν_g is the coupling parameter for collinear acoustic coupling and L_5 is the total length of the coupling grating.

Including dissipative loss, the matching condition (51) specialized to collinear acoustic coupling, is given by

$$(e^{-\kappa L_5})_{\text{opt}} = \frac{1}{4}(\mu_C + \mu_{Lg}) \tag{56}$$

where $\mu_C = 8g$ is the transducer loading on the resonator pair, and μ_{Lg} is the effective loading on each cavity due to all other mechanisms,

$$\mu_{Lg} = 8g_s + 4\epsilon_g + 4\frac{\alpha}{\kappa} + 4e^{-2\kappa L_1} \tag{57}$$

In deriving eq. (57), it is assumed that the outer gratings, G_1 and G_9, are identical.

Comparing eqs. (39) and (57), the expression for μ_{Lg} is similar to that for μ_L (for a single cavity) with the exceptions: (*i*) the grating-loss contribution is twice as large ($4\alpha/\kappa$ versus $2\alpha/\kappa$) because there are four effective reflection planes instead of two, and (*ii*) the excess loss ϵ_g is in

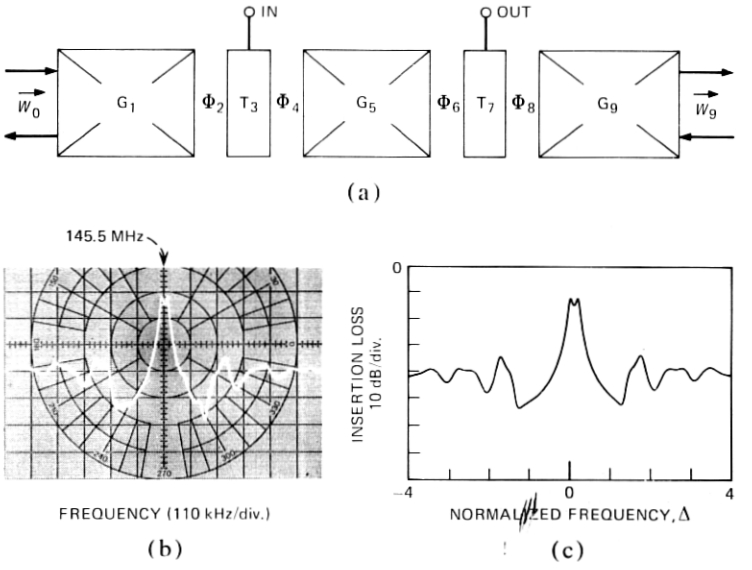

Fig. 9—(a) Diagram of an acoustically cascaded resonator-filter pair. (b) The electrical transmission spectrum in a 50 Ω system for an acoustically cascaded resonator-filter pair on YZ-$LiNbO_3$ with $L_1 = L_9 = 9.60$ mm, $L_5 = 7.296$ mm, $\Lambda = 12$ μm, $N_t = 5$ and an acoustic aperture of 50 wavelengths. (c) The calculated spectrum for the device in (b) using $\kappa = 3.3$ cm^{-1}, $\alpha/\kappa = 0.01$, $R_s = 12$ Ω, $\epsilon_g = 0.018$ and $\phi_2 = \phi_4 = \phi_6 = \phi_8 = 0.234\,\pi$ on resonance.

general different from the excess loss ϵ for a single cavity. In fact, the origins of the excess loss can be investigated, by comparing measured values of ϵ_g and ϵ. For example, if the excess loss is predominantly caused by the gratings, $\epsilon_g \simeq \epsilon$. If, however, the excess loss is transducer-associated, $\epsilon_g \approx \epsilon/2$ since there is only one transducer in each cavity in an acoustically coupled pair.

As an aid in design and data interpretation, the nomogram in Fig. 6 is directly applicable to matched acoustically coupled cavities when μ_{Lg} is substituted for μ_L.

The transmission spectrum of an acoustically coupled resonator pair is shown in Fig. 9b. The transducers and outer gratings are identical to those used in the single-cavity resonator in Fig. 5b. The experimental parameters have been estimated as described in the previous section, and the calculated response is shown in Fig. 9c. It is interesting to note that the value $\epsilon_g = 0.018 \approx \epsilon/2$ is found, providing further evidence that the excess loss is transducer associated on $LiNbO_3$.

VII. MULTISTRIP-COUPLED RESONATORS

Grating resonators can also be coupled using a directional (multistrip) coupler[6,7] as shown in Fig. 10a. A detailed analysis of the multistrip-coupled resonator pair from a scattering-matrix point of view has been

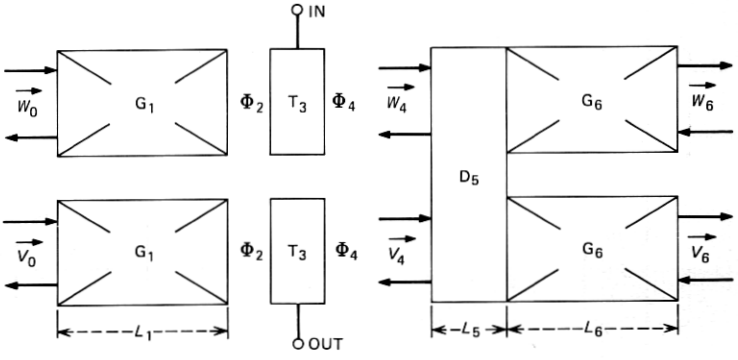

(a)

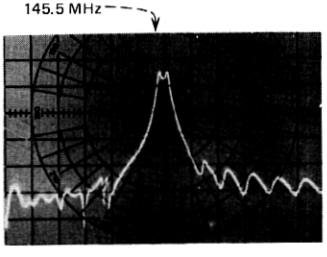

FREQUENCY (175 kHz/div.)

(b)

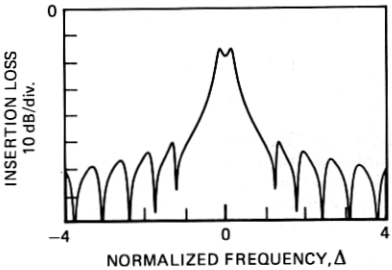

(c)

Fig. 10—(a) Diagram of a multistrip-coupled resonator-filter pair. (b) The electrical transmission spectrum in a 50 Ω system for a multistrip (5 μm strips, $L_5 = 90$ μm) coupled resonator-filter-pair on YZ-$LiNbO_3$ with $L_1 = L_6 = 9.60$ mm, $\Lambda = 12$ μm, $N_t = 5$ and an acoustic aperture in each track of 50 wavelengths. (c) The calculated transmission spectrum of the device in (b) with $q = 0.163$, $\kappa = 4.3$ cm^{-1}, $\alpha/\kappa = 0.01$, $R_s = 10$ Ω, $\epsilon_m = 0.047$, $\phi_2 = 0.25$ π and $\phi_4 = 9.89$ π on resonance.

given by Rosenberg and Coldren.[6] In this section we derive the coupling matrix ($\mathcal{C}_5$ in Fig. 7) for multistrip-coupled cavities.

The overall structure consists of two resonators in parallel connected by an ideal, directional coupler[27] described by the fourth-order vector equation

$$\begin{pmatrix} \mathbf{W}_4 \\ \mathbf{V}_4 \end{pmatrix} = \begin{pmatrix} \mathcal{P} & \mathcal{Q} \\ \mathcal{Q} & \mathcal{P} \end{pmatrix} \begin{pmatrix} \mathbf{W}_5 \\ \mathbf{V}_5 \end{pmatrix} \tag{58}$$

where

$$\mathcal{P} = \begin{pmatrix} p & 0 \\ 0 & p \end{pmatrix} \tag{59}$$

$$\mathcal{Q} = \begin{pmatrix} -jq & 0 \\ 0 & jq \end{pmatrix} \tag{60}$$

and

$$p^2 + q^2 = 1 \tag{61}$$

For simplicity, the frequency dependence of the propagation phase shifts through the multistrip coupler is ignored in eqs. (58)–(60).

Comparing Figs. 7 and 10a, the coupling element is the multistrip coupler in combination with the gratings G_6. The transmission between $\mathbf{W}_4$ in the upper track and $\mathbf{V}_4$ in the lower track can be treated as a two-port cascade element. Thus, the 2×2 matrix $\mathcal{D}$ satisfying

$$\begin{pmatrix} w_4^+ \\ w_4^- \end{pmatrix} = \mathcal{D} \begin{pmatrix} v_4^- \\ v_4^+ \end{pmatrix} \tag{62}$$

becomes the coupling matrix for multistrip-coupled cavities.

To solve for $\mathcal{D}$, the appropriate acoustic boundary conditions are

$$w_6^- = v_6^- = 0 \tag{63}$$

and the resulting matrix is

$$\mathcal{D} = \frac{j}{2pq} \begin{pmatrix} -\dfrac{1}{\Gamma_6} & (p^2 - q^2) \\ -(p^2 - q^2) & \Gamma_6 \end{pmatrix} \tag{64}$$

where Γ_6 is the reflection coefficient of the gratings, G_6.

Near resonance ($|\Delta| \ll 1$), Γ_6 can be expanded as in eq. (14), and for $\exp(\kappa L_6) \gg 1$, eq. (64) becomes

$$\mathcal{D} = \frac{1}{\nu_m} \mathcal{A} \begin{bmatrix} e^{j\Delta} & j\sqrt{1 - \nu_m^2} \\ -j\sqrt{1 - \nu_m^2} & e^{-j\Delta} \end{bmatrix} \mathcal{A} \tag{65}$$

where ν_m is the coupling parameter for multistrip-coupled cavities

$$\nu_m = 2q\sqrt{1 - q^2} \tag{66}$$

and $L_{\text{eff}} \approx 1/2\kappa$ since the length of the multistrip coupler is neglected. The loss matrix $\mathcal{A}$ in eq. (65) has the same form as that given for a single grating in (14b), but any excess loss due to the multistrip coupler must now be included. Thus, the matching condition for multistrip-coupled cavities becomes

$$q_{\text{opt}} = \frac{\mu_C + \mu_{Lm}}{\sqrt{16 + (\mu_C + \mu_{Lm})^2}} \tag{67}$$

where μ_{Lm} is the single-transit power loss of the resonator pair (excluding transducer coupling):

$$\mu_{Lm} = 8g_s + 4\epsilon_m + 4\frac{\alpha}{\kappa} + 4e^{-2\kappa L_6} \tag{68}$$

The excess loss ϵ_m now includes additional losses suffered due to the multistrip coupler.

As pointed out by Rosenberg,[6] far away from resonance ($|\Delta| \gg 1$) the multistrip-coupled structure has low out-of-band transmission, since the path connecting input and output requires a reflection from a grating. Quantitatively, from eq. (64).

$$\left|\frac{v_4^-}{w_4^+}\right|^2 = 4\nu_m^2 |\Gamma_6(\Delta)|^2 \tag{69}$$

As indicated by eq. (69), the effective cavity-coupling is directly proportional to Γ_6. Thus, the out-of-band transmission of a multistrip-coupled pair is low and can be suppressed to arbitrarily small values by using sidelobe-free apodized gratings.[28]

The nomogram in Fig. 6 can be used for matched, multistrip-coupled cavities when μ_{Lm} is substituted for μ_L, and the ordinate for out-of-band transmission is multiplied by $4\nu_m^2|\Gamma_6|^2$.

In Fig. 10b is shown the experimental transmission spectrum of a multistrip-coupled device, and in Fig. 10c is shown the spectrum for the same device calculated using (64) and the parameters given in the caption. The high resonant insertion loss (15 dB) is due to the large cavity perturbations ($\epsilon_m = 0.047$) caused both by the transducers and multistrip coupler. The distortion in the sidelobe response is due to slight nonuniformities in the gratings and direct capacitive coupling between the input and output transducers (RF feedthrough).

VIII. TRANSDUCER-COUPLED RESONATORS

The general scheme for using transducers to electrically couple two resonators is depicted in Fig. 11a. The coupling structure is topologically similar to the multistrip-coupled case, but with the important advantage that an electrical coupling network can be inserted between the resonators if desired. In general, both passive and active electrical circuit components can be employed so that passband shaping and amplification/attenuation can be performed in the coupling network. Thus, the electrically coupled configuration offers more design flexibility than either the acoustic cascade or directionally coupled configurations.

To gain an insight into the performance of electrically coupled resonators, we examine the important case[9,10] where the coupling network is simply a shunt susceptance $j\chi$. The coupling structure (transducers T_5 in combination with gratings G_7 and shunt susceptance $j\chi$) is described by the electrical coupling matrix $\mathscr{E}$ satisfying

$$\begin{pmatrix} w_4^+ \\ w_4^- \end{pmatrix} = \mathscr{E} \begin{pmatrix} v_4^- \\ v_4^+ \end{pmatrix} \tag{70}$$

Using the acoustic boundary conditions (as for the multistrip-coupled structure)

$$w_7^- = v_7^- = 0 \tag{71}$$

and assuming the two coupling transducers are identical, with N_t electrodes, the matrix $\mathcal{E}$ is found to be

$$\mathcal{E} = \frac{-2j(-1)^{N_t}Q_t}{(1+r)^2}\begin{bmatrix} 1 - j\left(\dfrac{1+r}{Q_t}\right) & r + j\left(\dfrac{1-r^2}{2Q_t}\right) \\ -r - j\left(\dfrac{1-r^2}{2Q_t}\right) & -r^2 + j\left(\dfrac{r(1+r)}{Q_t}\right) \end{bmatrix} \tag{72}$$

where $r = j\Gamma_7$, Γ_7 is the reflection coefficient of gratings G_7, and Q_t is the effective radiation Q of the cavity-coupling transducers:

$$Q_t = (\omega C_T + \chi/2)/G_r \tag{73}$$

The quantities C_T and G_r are the transducer static capacitance and radiation conductance, respectively. For clarity of exposition, in deriving eq. (72), the transducer length is assumed small compared to energy penetration depth in the gratings ($\theta_t \approx 0$) and the series resistance is neglected ($R_s = 0$). In eq. (72), the loss due to series resistance in the cavity-coupling transducers T_5 can be mathematically included in the grating loss coefficient as done for the losses in the multistrip coupler in Section VII.

For the electrical coupling structure, the phase shifts $\phi_6 = \pi/4$ must be included between the coupling transducers and the gratings G_7 in order to obtain optimum coupling of the transducers to the cavity standing-wave-pattern. Further, as noted by Matthaei *et al.*,[10] the coupling transducers introduce a small phase shift due to the finite value of Q_t. Thus, expanding (72) for $|\Delta| \ll 1$ and $\exp(\kappa L_7) \gg Q_t$, the matrix $\mathcal{E}$ is given by

$$\mathcal{E} = -(-1)^{N_t}\frac{1}{\nu_t}\mathcal{A}\begin{bmatrix} e^{j(\Delta+\phi_{ex})} & j\sqrt{1-\nu_t^2} \\ -j\sqrt{1-\nu_t^2} & e^{-j(\Delta+\phi_{ex})} \end{bmatrix}\mathcal{A} \tag{74}$$

where the matrices $\mathcal{A}$ account for all dissipative cavity losses due to gratings and transducers T_5, and the constant excess phase shift ϕ_{ex} is given by

$$\phi_{ex} = \pi/2 - 2/Q_t \tag{75}$$

The quantity ν_t is the cavity-coupling parameter for transducer coupling,

$$\nu_t = \frac{2Q_t}{Q_t^2 + 1} \tag{76}$$

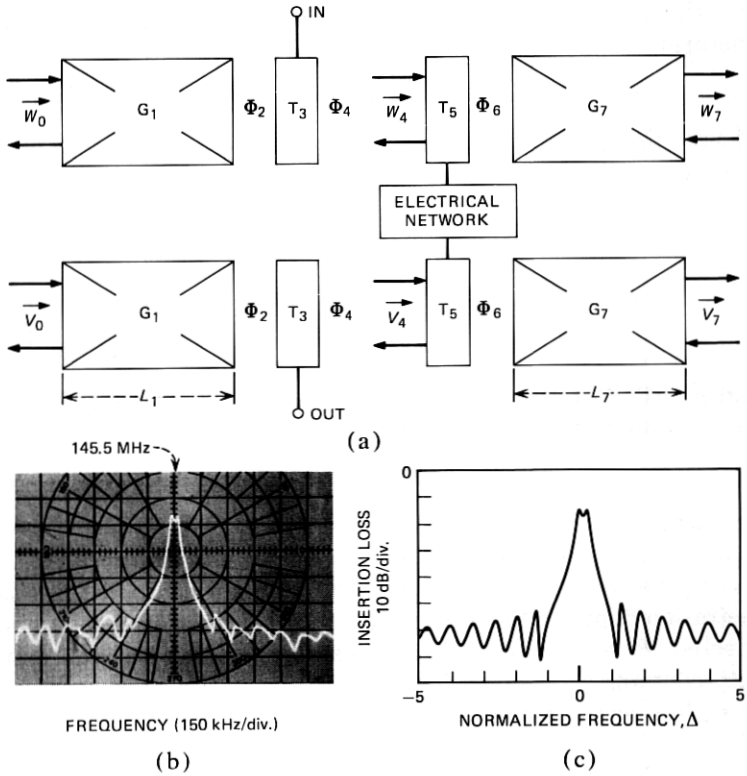

Fig. 11—(a) Diagram of a transducer-coupled resonator-filter pair. (b) The electrical transmission spectrum in a 50 Ω system of an electrically coupled, resonator-filter pair on YZ-$LiNbO_3$ with optimally placed transducers with $N_t = 5$, $L_1 = L_7 = 9.60$ mm, $\Lambda = 12$ μm and an acoustic aperture in each track of 50 wavelengths. (c) The calculated spectrum of the device in (b) with $Q_t = 6.69$, $\kappa = 4.0\ \text{cm}^{-1}$, $\alpha/\kappa = 0.01$, $R_s = 11\ \Omega$, $\epsilon_t = 0.047$, and $\phi_4 = 10\pi$ on resonance.

Here again, L_{eff} in (49) is given by the penetration depth $(1/2\kappa)$ into the grating since the transducer length has been ignored. The matching condition for transducer-coupled cavities becomes

$$(Q_t)_{\text{opt}} = \frac{4}{\mu_C + \mu_{Lt}} \tag{77}$$

where μ_{Lt} is the single-transit power loss of the resonator pair (excluding loading by the external circuit),

$$\mu_{Lt} = 8g_s + 4\epsilon_t + 4\frac{\alpha}{\kappa} + 4e^{-2\kappa L_7} \tag{78}$$

The excess loss ϵ_t accounts for all additional losses due to the cavity-coupling transducers as well as the excess loss from the input-output

transducers, and the term $8g_s$ is due to the input-output transducers T_3.

Outside the grating stop-band ($|\Delta| \gg 1$), the power transmission $|v_4^-/w_4^+|^2$ through the coupling elements tends to the limit

$$\left|\frac{v_4^-}{w_4^+}\right|^2 \approx \left(\frac{\nu_t}{4}\right)^2 \tag{79}$$

The out-of-band transmission of the transducer-coupled configuration is therefore lower than with collinear acoustic coupling but is still higher than the out-of-band level for multistrip-coupled resonators [see (69)].

The resonator nomograph in Fig. 6 can be used for matched, transducer-coupled resonators when μ_{Lt} is substituted for μ_L, and the ordinate for out-of-band transmission is multiplied by $(\nu_t/4)^2$.

In Fig. 11b, the experimental transmission spectrum of a pair of transducer-coupled cavities is shown, and the theoretical response of the same device calculated using (72) and the parameters given in the caption is shown in Fig. 11c. The excess loss ϵ_t is about the same as ϵ for a single-cavity resonator, as would be expected. As for the multistrip-coupled pair, the distortion in the sidelobe response is caused by grating nonuniformities and RF feedthrough.

IX. SUMMARY AND CONCLUSIONS

The major results derived in this paper are summarized in Table I. Gratings and small pieces of transmission line are the fundamental elements for SAW resonators. Using coupled-mode theory, gratings and transmission lines are described by 2×2 transmission matrices. Resonators and combinations of resonators can be analyzed simply by multiplying together a sequence of transmission matrices. A matrix-multiplication algorithm is also presented for analyzing bandpass filters with intracavity transducers.

To form multipole filters, several resonators can be coupled together using one or more of the three mechanisms: (*i*) collinear acoustic coupling, (*ii*) multistrip coupling, or (*iii*) transducer coupling. Near the resonant frequency all three mechanisms are mathematically equivalent and can be used interchangeably in passband synthesis applications. Far off the resonant frequency, the three mechanisms have quite different sidelobe suppression characteristics.

The essential properties of the three coupling mechanisms are illustrated in Fig. 12. The calculated transmission spectra for three different coupled resonator pairs are shown. In each case, the cavities are of identical length and are coupled to the same degree (same value of ν) with only the cavity-coupling mechanism being changed from case to case. All three spectra have nearly the same passband shape, but the electri-

Table I—Summary of resonator elements

Element	Schematic diagram	Simplified, near-resonance description	Relevant equations
Grating		$\begin{bmatrix} w_{i-1}^+ \\ w_{i-1}^- \end{bmatrix} = \frac{1}{\nu_g} \begin{bmatrix} e^{j\Delta} & j\sqrt{1-\nu_g^2} \\ -j\sqrt{1-\nu_g^2} & e^{-j\Delta} \end{bmatrix} \begin{bmatrix} w_i^+ \\ w_i^- \end{bmatrix}$ $\nu_g = \operatorname{sech}(\kappa L)$	(8), (14) (82)
Transmission line	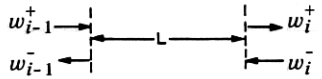	$\begin{bmatrix} w_{i-1}^+ \\ w_{i-1}^- \end{bmatrix} = \begin{bmatrix} e^{j\beta L} & 0 \\ 0 & e^{-j\beta L} \end{bmatrix} \begin{bmatrix} w_i^+ \\ w_i^- \end{bmatrix}$	(13)
Transducer	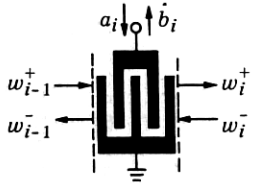	$\begin{bmatrix} w_{i-1}^+ \\ w_{i-1}^- \\ b_i \end{bmatrix} = (-1)^{N_t} \begin{bmatrix} 1+g & -g & (-1)^{N_t}\sqrt{2g} \\ g & 1-g & (-1)^{N_t}\sqrt{2g} \\ \sqrt{2g} & -\sqrt{2g} & (-1)^{N_t} \end{bmatrix} \begin{bmatrix} w_i^+ \\ w_i^- \\ a_i \end{bmatrix}$	(25), (26), (32), (84)
Multistrip cavity coupler	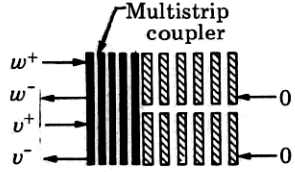	$\begin{bmatrix} w^+ \\ w^- \end{bmatrix} = \frac{1}{\nu_m} \begin{bmatrix} e^{j\Delta} & j\sqrt{1-\nu_m^2} \\ -j\sqrt{1-\nu_m^2} & e^{-j\Delta} \end{bmatrix} \begin{bmatrix} v^- \\ v^+ \end{bmatrix}$ $\nu_m = 2q$	(64), (65)
Transducer cavity coupler	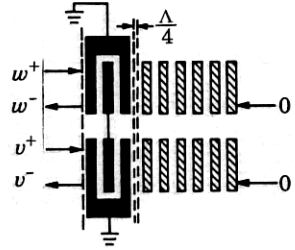	$\begin{bmatrix} w^+ \\ w^- \end{bmatrix} = \frac{1}{\nu_t} \begin{bmatrix} e^{j(\Delta+\phi_{ex})} & j\sqrt{1-\nu_t^2} \\ -j\sqrt{1-\nu_t^2} & e^{-j(\Delta+\phi_{ex})} \end{bmatrix} \begin{bmatrix} v^- \\ v^+ \end{bmatrix}$ $\nu_t = 2/Q_t$ $\phi_{ex} = \pi/2 - \nu_t$	(72), (74), (75), (76)

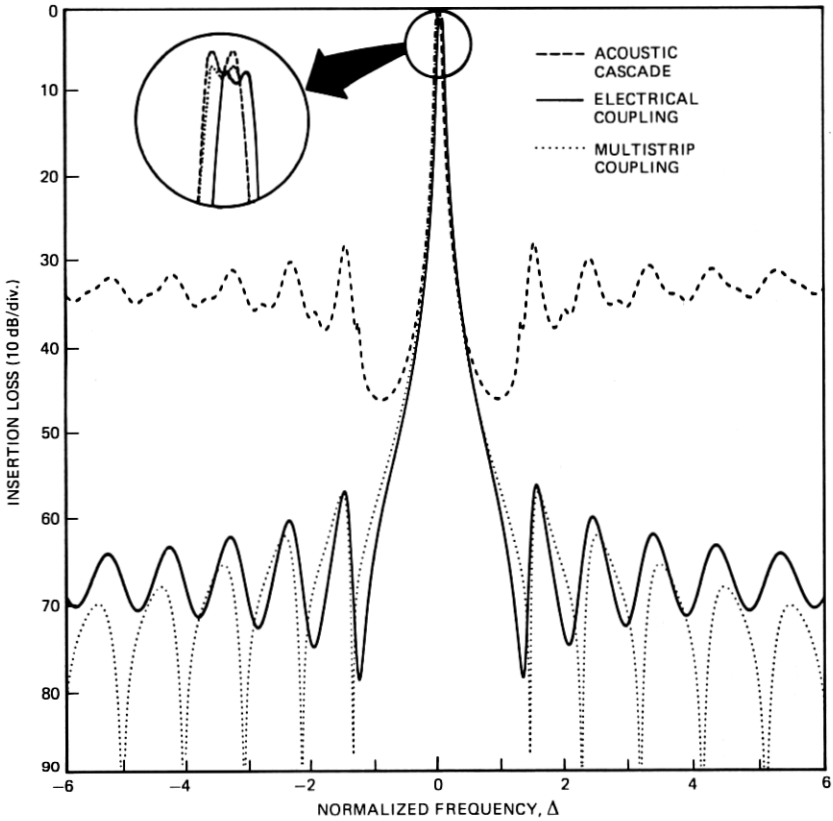

Fig. 12—The calculated transmission spectra of three equivalent resonator-filter pairs on YZ-$LiNbO_3$, each using a different cavity-coupling mechanism. In each case, the devices are assumed lossless and the outer gratings are 800 periods long with $\Lambda = 12\ \mu m$ and $\kappa = 3.27\ cm^{-1}$. The transducers have $N_t = 5$ with an acoustic aperture of 100 wavelengths. The degree of cavity coupling is the same in each case with $\nu_g = \nu_m = \nu_t = 0.077$.

cally coupled pair resonates at a higher frequency than the others due to the phase shift introduced by the cavity-coupling transducers. The multistrip and electrically coupled cavities have a slightly greater resonant insertion loss than the acoustic cascade because some energy is lost through the end gratings G_6 in Fig. 10 and G_7 in Fig. 11. The sidelobe levels are highest for the acoustic cascade and progressively lower for transducer and then multistrip coupling.

For the synthesis of multipole filters each coupling mechanism has unique advantages so that a combination of two or more coupling mechanisms will probably be optimal. The acoustic cascade is particularly easy to design because coupling between cavities can be accomplished without disturbing the intrinsic cavity properties. That is, there

are no velocity perturbations, ohmic losses, or spurious reflections introduced into the cavity by the coupling structure.

Transducer coupling allows the flexibility of using an external electrical network in addition to the additional sidelobe suppression mentioned above. The external network can be used to contribute to passband shaping and as a convenient means for post-fabrication trimming of device performance.

Finally, the multistrip coupler offers the lowest sidelobe levels and the technological advantage that no critical alignment of the coupler within the cavity is required (as is the case for transducers).

Beginning with the gross properties of the various coupling mechanisms discussed above and emphasized in Fig. 12, the simple matrices given in Table I can be used to obtain first-order results for a wide variety of filter configurations. More precise results can then be obtained using the exact expressions given earlier in the text. Thus, the analytical techniques presented in this paper should provide a sound basis for developing a synthesis procedure for multipole SAW resonator filters.

ACKNOWLEDGMENTS

The authors wish to acknowledge the valuable technical assistance of L. L. Buhl in device fabrication; of R. H. Bosworth in photomask layout; and of M. J. Madden in the numerical computations. The authors also benefited from numerous discussions with G. D. Boyd, L. A. Coldren, and R. L. Rosenberg which stimulated several aspects of this work.

APPENDIX A—TRANSMISSION MATRIX FOR LOSSY GRATINGS

In this appendix a general grating transmission matrix is derived which includes a propagation attenuation and allows for an arbitrary choice of reference planes.

As in Section II, the grating extends from $x = -L$ to $x = 0$. The velocity perturbation is now generalized to allow an arbitrary phase shift, θ, of the grating with respect to the x axis:

$$v(x) = v_0 - \frac{\Delta v}{2} \cos (Kx + \theta) \tag{80}$$

The scalar wave equation is modified to

$$\frac{d^2\Psi}{dx^2} + \left(\frac{\omega^2}{v^2(x)} - j\frac{2\omega\alpha}{v(x)}\right)\Psi = 0 \tag{81}$$

which includes a propagation attenuation coefficient, α. The grating transmission matrix is found in the manner described in Section II. For

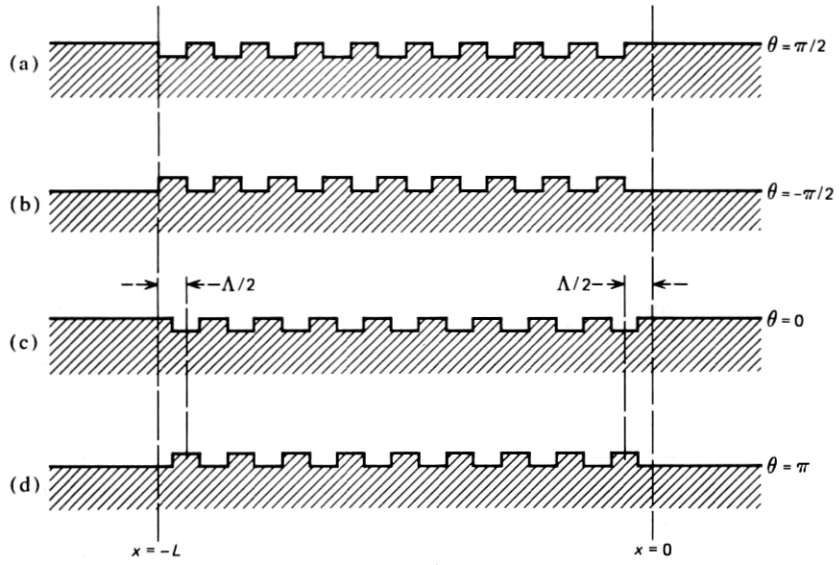

Fig. 13—Location of reference planes and phase angles, θ, for YZ-$LiNbO_3$ and ST quartz surface-deformation gratings: (a) step-down grating with reference plane at the first down-step, (b) step-up grating with reference plane at the first up-step, (c) step-down grating with symmetrically placed reference planes; (d) step-up grating with symmetrically placed reference planes.

the narrowband approximation, $\beta/\beta_0 \approx 1$, the transmission matrix becomes

$$\mathcal{G} = \frac{\kappa}{\sigma}\cosh(\sigma L) \times \begin{bmatrix} \left[\frac{\sigma}{\kappa} + j\left(\frac{\delta - j\alpha}{\kappa}\right)\tanh(\sigma L)\right] e^{j\beta_0 L} & je^{-j\theta}\tanh(\sigma L)e^{j\beta_0 L} \\ -je^{j\theta}\tanh(\sigma L)e^{-j\beta_0 L} & \left[\frac{\sigma}{\kappa} - j\left(\frac{\delta - j\alpha}{\kappa}\right)\tanh(\sigma L)\right] e^{-j\beta_0 L} \end{bmatrix} \quad (82)$$

where

$$\sigma = [\kappa^2 - (\delta - j\alpha)^2]^{1/2}$$

This matrix reduces to eq. (8b) when α and θ are set equal to zero.

It is shown in Section II that the magnitude of the grating reflection coefficient provides a means of determining the coupling coefficient. Similarly, the phase of the reflection coefficient specifies the parameter

θ for a particular choice of reference planes. For a lossless grating an integral number of periods long, the reflection coefficient at the Bragg frequency is

$$\Gamma(0) = -je^{+j\theta} \tanh(\kappa L) \tag{83}$$

Thus, when the reference planes of a grating are spaced by an integral number of periods, one need only measure the phase of the reflection coefficient at the Bragg frequency in order to determine θ. For example, consider surface corrugation gratings of the step-down and step-up type as shown in Fig. 13. The experimentally observed optimum transducer placement has shown for both YZ-$LiNbO_3$[29,30] and ST-quartz[17,30] that the electric potential, Ψ, is a maximum at the edge of a step-down grating, and a minimum at the step-up grating edge. Accordingly, for reference planes shown in Fig. 13a, $\theta = +\pi/2$ for a step-down grating and in Fig. 13b, $\theta = -\pi/2$ for a step-up grating. Similarly, for any type of grating and choice of reference plane, θ can be determined from knowledge of the optimum transducer[25] location which gives the position of the potential maximum. For the case of step-down gratings, $\theta = 0$ corresponds to the symmetrical choice of reference planes as shown in Fig. 13c. A symmetrical choice of reference planes for a step-up grating is as shown in Fig. 13d, which requires $\theta = \pi$. In this paper we assume the reference planes have been chosen such that $\theta = 0$ for mathematical simplicity.

APPENDIX II—TRANSDUCER TRANSMISSION MATRIX AND RESONATOR-ANALYSIS ALGORITHM

The transmission matrix $\mathcal{T}$ of an IDT can be found by manipulating the well-known admittance matrix[23,24] based on a Mason equivalent-circuit model. Using the results of Smith *et al.*,[23] and including an effective series electrode resistance, R_s, $\mathcal{T}$ is given by

$$\mathcal{T} = s\begin{pmatrix} (1+t_0)e^{j\theta_t} & -t_0 & st_{13} \\ t_0 & (1-t_0)e^{-j\theta_t} & st_{13}e^{-j\theta_t} \\ t_{13} & -t_{13}e^{-j\theta_t} & st_{33} \end{pmatrix} \tag{84}$$

where

$$t_0 = \frac{G_r(R_s + Z_e)}{1 + j\theta_e} \tag{85}$$

$$t_{13} = \frac{\sqrt{2G_rZ_e}}{1 + j\theta_e} e^{j\theta_t/2} \tag{86}$$

$$t_{33} = 1 - \frac{2j\theta_c}{1 + j\theta_e} \tag{87}$$

$$s = (-1)^{N_t} \tag{88}$$

N_t = number of electrodes in the transducer

$$\theta_t = N_t \Lambda \delta \tag{89}$$

G_r = transducer radiation conductance

$$\theta_c = \omega C_T (R_s + Z_e) \tag{90}$$

$$\theta_e = (\omega C_T + B_r)(R_s + Z_e) \tag{91}$$

$$C_T = (N_t - 1) C_s / 2 \tag{92}$$

B_r = transducer radiation susceptance

C_s = static capacitance/electrode pair

For uniform transducers,[23,31]

$$G_r \approx 2G_0 (N_t - 1)^2 \left[\frac{\sin\left(\frac{\theta_t}{2}\right)}{\frac{\theta_t}{2}} \right]^2 \tag{93}$$

$$G_0 = k_c^2 C_s \omega / 2\pi \tag{94}$$

k_c^2 = electromechanical coupling constant

$$B_r \simeq 4G_0 (N_t - 1)^2 \frac{\sin(\theta_t) - \theta_t}{\theta_t^2} \tag{95}$$

Using the transducer description in eq. (84), we develop an algorithm for analyzing coupled resonators with intracavity transducers. Consider the general cascaded-resonator structure in Fig. 7. The input signal is applied to transducer T_3 which is separated by phase shift Φ_2 from grating G_1. The output is taken from transducer T_7 which is separated by phase-shift Φ_8 from grating G_9. The element C_5 is a generalized coupling element that can be composed of gratings, transducers, phase shifts, and multistrip couplers. The coupling element C_5 is described by the 2×2 transmission matrix $\mathscr{C}_5$. Specific examples of the matrix $\mathscr{C}_5$ are given in the main text for: (*i*) a single-cavity, two-port resonator, (*ii*) acoustically cascaded resonators, (*iii*) multistrip-coupled resonators, and (*iv*) electrically coupled resonators.

From eq. (27), the acoustic amplitudes associated with transducer T_3 can be expressed

$$\mathbf{W}_2 = t_3 \mathbf{W}_3 + a_3 \boldsymbol{\tau}_3 \tag{96}$$

Vector equation (96) is actually two equations with four unknowns $w_2^{\pm}$, $w_3^{\pm}$. Two further equations are obtained from the boundary conditions

expressing the fact that there are no acoustic waves externally incident on the resonator

$$w_0^+ = w_9^- = 0 \tag{97}$$

Next, the boundary conditions can be referred to the reference planes of transducer T_3:

$$\mathbf{W}_0 = \mathcal{G}_1\Phi_2\mathbf{W}_2 \tag{98}$$

$$\mathbf{W}_3 = \mathcal{C}_5\Phi_6 t_7\Phi_8\mathcal{G}_9\mathbf{W}_9 \tag{99}$$

where it is assumed transducer T_7 is connected to a matched load (i.e., $a_7 = 0$).

Combining eqs. (96), (98), and (99), the outward propagating acoustic waves w_9^+ and w_0^- are specified in terms of the electrical input, a_3,

$$\begin{pmatrix} 0 \\ w_0^- \end{pmatrix} = \mathcal{M}\begin{pmatrix} w_9^+ \\ 0 \end{pmatrix} + a_3\mathcal{G}_1\Phi_2\tau_3 \tag{100}$$

where $\mathcal{M}$ is the overall acoustic transmission matrix

$$\mathcal{M} = \mathcal{G}_1\Phi_2 t_3\Phi_4\mathcal{C}_5\Phi_6 t_7\Phi_8\mathcal{G}_9 \tag{101}$$

The vector $\mathbf{W}_7$ is next found from $\mathbf{W}_9$,

$$\mathbf{W}_7 = \Phi_8\mathcal{G}_9\mathbf{W}_9 \tag{102}$$

Finally, from eq. (30) the electrical output amplitude b_7 is given by

$$b_7 = \tau_7' \cdot \mathbf{W}_7 \tag{103}$$

The analysis leading up to eq. (103) is essentially a derivation of a general algorithm for finding the two-port, electrical-transmission characteristics of a grating resonator with an arbitrary coupling element C_5. The algorithm can therefore be applied to single-cavity resonators as well as more complex, multipole structures.

The analysis can be further simplified by considering transducer T_3 in combination with grating G_1 as an "input" coupler described by the matrix $\mathcal{C}^{IN}$

$$\begin{pmatrix} a_3 \\ b_3 \end{pmatrix} = \mathcal{C}^{IN}\begin{pmatrix} w_3^+ \\ w_3^- \end{pmatrix} \tag{104}$$

Similarly, transducer T_7 and grating G_9 form an "output" coupler described by $\mathcal{C}^{OUT}$

$$\begin{pmatrix} w_6^+ \\ w_6^- \end{pmatrix} = \mathcal{C}^{OUT}\begin{pmatrix} b_7 \\ a_7 \end{pmatrix} \tag{105}$$

The overall electrical transfer function is then found from

$$\begin{pmatrix} a_3 \\ b_3 \end{pmatrix} = \mathcal{C}^{IN}\Phi_4\mathcal{C}_5\Phi_6\mathcal{C}^{OUT}\begin{pmatrix} b_7 \\ a_7 \end{pmatrix} \tag{106}$$

For optimal transducer placement and, for simplicity, neglecting R_s and θ_t, $\mathcal{C}^{IN}$ and $\mathcal{C}^{OUT}$ are given by

$$\mathcal{C}^{IN} = \frac{-(-1)^{N_t}}{\sqrt{2g}} \begin{bmatrix} c_{11} & c_{12} \\ c_{21} & c_{22} \end{bmatrix} \tag{107}$$

and

$$\mathcal{C}^{OUT} = \frac{1}{\sqrt{2g}} \begin{bmatrix} c_{11} & -c_{21} \\ -c_{12} & c_{22} \end{bmatrix} \tag{108}$$

where

$$c_{11} = g + \frac{1 + j\theta_e}{1 + r} \tag{109}$$

$$c_{12} = -g + \frac{(1 + j\theta_e)r}{1 + r} \tag{110}$$

$$c_{21} = -g + \frac{1 - j\theta_e}{1 + r} \tag{111}$$

$$c_{22} = g + \frac{(1 - j\theta_e)r}{1 + r} \tag{112}$$

$$g = G_r Z_e$$

$$r = j\Gamma$$

and Γ is the reflection coefficient of the appropriate grating (G_1 or G_9).

REFERENCES

1. D. T. Bell and R. C. M. Li, "Surface-Acoustic-Wave Resonators," Proc. IEEE, *64* (May 1976), pp. 711–721.
2. C. S. Hartmann and R. C. Rosenfeld, U.S. Patent No. 3,886,504, May 1975.
3. H. A. Haus and R. V. Schmidt, "Transmission Response of Cascaded Gratings," IEEE Trans. Son. Ultrason., *SU-24* (March 1977), pp. 94–101.
4. P. S. Cross, R. V. Schmidt, and H. A. Haus, "Acoustically Cascaded SAW Resonator Filters," 1976 IEEE Ultrason. Symp. Proc., September 1976, pp. 277–280.
5. E. J. Staples, Proc. 30th Annual Symposium on Frequency Control, U. S. Army Electronics Command, Fort Monmouth, New Jersey, June 1976, pp. 322–327.
6. R. L. Rosenberg and L. A. Coldren, "Reflection-Dependent Coupling Between Grating Resonators," 1976 IEEE Ultrason Symp. Proc., September 1976, pp. 281–286.
7. M. Redwood, R. B. Topolevsky, R. F. Mitchell, and J. S. Palfreeman, "Coupled-Resonator Acoustic-Surface-Wave Filter," Electron. Lett., *11*, No. 12 (June 12, 1975), pp. 253–254.
8. P. S. Cross, R. S. Smith, and W. H. Haydl, "Electrically Cascaded Surface-Acoustic-Wave Resonator Filter," Electron. Lett., *11*, No. 11 (May 29, 1975), pp. 244–245.
9. W. R. Shreve, "Surface-Wave Two-Port Resonator Equivalent Circuit," 1975 IEEE Ultrasonics Symp. Proc., September 1975, pp. 295–298.
10. G. L. Matthaei, B. P. O'Shaughnessy, and F. Barman, "Relations for Analysis and Design of Surface Wave Resonators," IEEE Trans. Son. Ultrason. *SU-23*, March 1976, pp. 99–107.
11. H. Kogelnik, "Coupled Wave Theory for Thick Hologram Gratings," B.S.T.J., *48*, No. 9 (November 1969), pp. 2909–2947.

12. H. Kogelnik and C. V. Shank, "Coupled-Wave Theory of Distributed Feedback Lasers," J. Appl. Phys., *43*, No. 5 (May 1972), pp. 2327–2335.
13. H. A. Haus and C. V. Shank, "Antisymmetric Taper of Distributed Feedback Lasers," IEEE J. Quantum Electron., *QE-12*, No. 9 (September 1976), pp. 532–538.
14. R. V. Schmidt, "Acoustic Surface Wave Velocity Perturbations in $LiNbO_3$ by Diffusion of Metals," Appl. Phys. Lett., *27*, No. 1 (July 1, 1975), pp. 8–10.
15. R. C. M. Li, R. C. Williamson, D. C. Flanders, and J. A. Alusow, "On the Performance and Limitations of the Surface-Wave Resonator Using Grooved Reflectors," 1974 IEEE Ultrason. Symp. Proc., November 1974, pp. 257–262.
16. R. C. M. Li, J. A. Alusow, and R. C. Williamson, "Experimental Exploration of the Limits of Achievable Q of the Grooved Surface Wave Resonator," 1975 IEEE Ultrason. Symp. Proc., September 1975, pp. 279–283.
17. L. A. Coldren and R. L. Rosenberg, "Scattering Matrix Approach to SAW Resonators," 1976 IEEE Ultrason. Symp. Proc., September, 1976, pp. 266–271, and L. A. Coldren, "Characteristics of Surface Acoustic Wave Resonators Obtained from Cavity Analysis," IEEE Trans. Son. Ultrason, May 1977, pp. 212–217.
18. R. C. M. Li, J. A. Alusow, and R. C. Williamson, "Surface-Wave Resonators Using Grooved Reflectors," Proc. 29th Annual Freq. Control Symp., U.S. Army Electronics Command, Ft. Monmouth, New Jersey, May, 1975, pp. 167–176.
19. L. Storch, "The Transmission Matrix of N Alike Cascaded Networks," AIEE Trans. (Communications and Electronics), *73*, January 1955, pp. 616–618.
20. W. H. Haydl and P. S. Cross, "Fine Tuning of Surface-Acoustic-Wave Resonator Filters with Metallization Thickness," Electron. Lett., *11*, No. 12 (June 12, 1975), pp. 252–253.
21. E. J. Staples, J. S. Schoenwald, R. C. Rosenfeld, and C. S. Hartmann, "UHF Surface Acoustic Wave Resonators," 1974 IEEE Ultrason. Symp. Proc., November 1974, pp. 245–252.
22. G. L. Matthaei, F. Barman, E. B. Savage, and B. O. O'Shaughnessy, "A Study of the Properties and Potential Application of Acoustic-Surface-Wave Resonators," 1975 IEEE Ultrason. Symp. Proc., September 1975, pp. 284–289.
23. W. R. Smith, H. M. Gerard, J. H. Collins, T. M. Reeder, and H. J. Shaw, "Analysis of Interdigital Surface Wave Transducers by Use of an Equivalent Circuit Model," IEEE Trans. Microw. Theory Tech., *MTT-17*, November, 1969, pp. 850–873.
24. K. M. Lakin and T. R. Joseph, "Surface Wave Resonators," 1975 IEEE Ultrason. Symp. Proc., September 1975, pp. 269–278.
25. P. S. Cross, "Properties of Reflective Arrays for Surface Acoustic Resonators," IEEE Trans. Son. Ultrason. *SU-23*, No. 4 (July 1976), pp. 255–262.
26. A. Ashkin, G. D. Boyd, and J. M. Dziedzic, "Resonant Optical Second Harmonic Generation and Mixing," IEEE Jour. Quantum Electron., *QE-2*, No. 6 (June 1966), pp. 109–124.
27. R. N. Ghose, *Microwave Circuit Theory and Analysis*, New York: McGraw-Hill, 1963, Chap. 10.
28. P. S. Cross and H. Kogelnik, "Sidelobe Suppression in Corrugated-Waveguide Filters," Opt. Lett., *1*, No. 1 (July 1977), pp. 43–45.
29. R. V. Schmidt and P. S. Cross—unpublished work.
30. W. H. Haydl, B. Dischler, and P. Hiesinger, "Multimode SAW Resonators—A Method to Study the Optimum Resonator Design," Proc. 1976 IEEE Ultrason. Symp., September 1976, pp. 287–296.
31. G. L. Matthaei, D. Y. Wong, and B. P. O'Shaughnessy, "Simplifications for the Analysis of Interdigital Surface-Wave Devices," IEEE Trans. Son. Ultrason., *SU-22*, No. 2 (March 1975), pp. 105–114.